High-pressure synthesis and characterization of the effective pseudospin $S = 1/2$ XY pyrochlores $R_2Pt_2O_7$ (R = Er, Yb)

Y. Q. Cai,[1] Q. Cui,[1] X. Li,[2] Z. L. Dun,[3] J. Ma,[3] C. dela Cruz,[4] Y. Y. Jiao,[1] J. Liao,[1] P. J. Sun,[1] Y. Q. Li,[1] J. S. Zhou,[2] J. B. Goodenough,[2] H. D. Zhou,[3] and J.-G. Cheng[1,*]

[1]*Beijing National Laboratory for Condensed Matter Physics and Institute of Physics, Chinese Academy of Sciences, Beijing 100190, China*

[2]*Materials Science and Engineering Program and Texas Materials Institute, University of Texas at Austin, Austin, Texas 78712, USA*

[3]*Department of Physics and Astronomy, University of Tennessee, Knoxville, Tennessee 37996, USA*

[4]*Quantum Condensed Matter Division, Oak Ridge National Laboratory, Oak Ridge, Tennessee 37831, USA*

(Received 13 December 2015; published 28 January 2016)

We report on the high-pressure syntheses and detailed characterizations of two effective pseudospin $S = 1/2$ XY pyrochlores $Er_2Pt_2O_7$ and $Yb_2Pt_2O_7$ via x-ray/neutron powder diffraction, dc and ac magnetic susceptibility, and specific-heat measurements down to 70 mK. We found that both compounds undergo long-range magnetic transitions at $T_{N,C} \approx 0.3$ K, which are ascribed to an antiferromagnetic- and ferromagnetic-type order for $Er_2Pt_2O_7$ and $Yb_2Pt_2O_7$, respectively, based on the field dependence of their transition temperatures as well as the systematic comparisons with other similar pyrochlores $R_2B_2O_7$ (R = Er, Yb; B = Sn, Ti, Ge). The observed T_N of $Er_2Pt_2O_7$ is much lower than that expected from the relationship of T_N versus the ionic radius of B^{4+} derived from the series of $Er_2B_2O_7$, while the T_C of $Yb_2Pt_2O_7$ is the highest among the series of ferromagnetic compounds $Yb_2B_2O_7$ (B = Sn, Pt, Ti). Given the monotonic variation of the lattice constant as a function of the B-cation size across these two series of $R_2B_2O_7$ (R = Er, Yb), the observed anomalous values of $T_{N,C}$ in the Pt-based XY pyrochlores imply that another important factor beyond the nearest-neighbor R-R distance is playing a role. In light of the anisotropic exchange interactions $J_{ex} = \{J_{zz}, J_{\pm}, J_{\pm\pm}, J_{z\pm}\}$ for the $S = 1/2$ XY pyrochlores, we have rationalized these observations by considering a weakened (enhanced) antiferromagnetic planar $J_{\pm}$ (ferromagnetic Ising-like J_{zz}) due to strong Pt $5d$-$O2p$ hybridization within the plane perpendicular to the local [111] direction.

DOI: 10.1103/PhysRevB.93.014443

I. INTRODUCTION

Pyrochlore oxides $R_2B_2O_7$,where R^{3+} stands for a rare-earth ion and B^{4+} for a nonmagnetic cation such as Sn^{4+} or Ti^{4+}, consist of an important family of geometrically frustrated magnets, which have been the focus of extensive investigations over recent decades [1]. In the cubic $R_2B_2O_7$ pyrochlores, the magnetic R^{3+} ions are situated on a network of corner-sharing tetrahedra and the exchange interactions are subjected to strong geometrical frustration. In addition, the significant local axial distortion around R^{3+} can create distinct single-ion anisotropy for different R^{3+} ions, such as the strong Ising character for Ho^{3+}, Dy^{3+}, and Tb^{3+}, and the XY-type Er^{3+} and Yb^{3+} moments. The combinations of single-ion anisotropy and frustrated exchange and dipolar interactions in these $R_2B_2O_7$ pyrochlores can give rise to a broad spectrum of magnetic phenomena, including the exotic order-by-disorder mechanism, spin ice, and spin liquid [1].

Research interest in these geometrically frustrated $R_2B_2O_7$ compounds has shifted in recent years from classical to quantum spin systems because the introduction of quantum fluctuations is expected to produce exotic magnetic ground states with unconventional spin excitations [2]. In this regard, Er- and Yb-based XY pyrochlores $R_2B_2O_7$ (R = Er, Yb) with effective pseudospins $S = 1/2$ and small magnetic moments based on a well-isolated Kramers doublet for the R^{3+} ions have been the subject of intense theoretical and experimental investigations during the last few years.

$Er_2Ti_2O_7$ exhibits a long-range antiferromagnetic order below $T_N = 1.17$ K [3], and the magnetic order with a noncoplanar ψ_2 structure has been argued to be driven by quantum fluctuations via an "order-by-disorder (OBD)" mechanism [3–8]. However, its sister compound $Er_2Sn_2O_7$ does not show any long-range magnetic order down to 50 mK [9,10]. In order to elucidate this dilemma, we recently synthesized a cubic $Er_2Ge_2O_7$ compound under high-pressure and high-temperature (HPHT) conditions and investigated systematically the influence of chemical pressure on the magnetic ground states of these Er-based XY pyrochlore antiferromagnets [11,12]. It was found that $Er_2Ge_2O_7$ with a much reduced interatomic distance orders antiferromagnetically below $T_N = 1.4$ K with a possible ψ_3 structure [12] in contrast to the ψ_2 structure observed in $Er_2Ti_2O_7$. In light of the phase diagram for the $S = 1/2$ XY pyrochlore antiferromagnets with anisotropic exchange interactions $J_{ex} = \{J_{zz}, J_{\pm}, J_{\pm\pm}, J_{z\pm}\}$, we have rationalized the evolution of the magnetic ground states of $Er_2B_2O_7$ (B = Sn, Ti, Ge) from the Palmer-Chalker (PC) ψ_4 state to ψ_2, and finally to ψ_3 via considering the progressively enhanced XY-type exchange interaction $J_{\pm}$ under chemical pressure [8,12].

Despite the similar XY anisotropy for the Yb^{3+} moment [13], the local [111] Ising-like ferromagnetic exchange interaction J_{zz} is considerably larger than the XY planar interaction $J_{\pm}$ in $Yb_2Ti_2O_7$, making it a promising candidate for a quantum spin ice [14,15]. Existing experimental results have established that both $Yb_2Sn_2O_7$ and $Yb_2Ti_2O_7$ cubic pyrochlores actually develop a long-range magnetic order below $T_C = 0.11$–0.15 K (Sn) [16,17] and 0.21–0.26 K (Ti) [18,19] through a first-order-like transition featuring a sharp

*jgcheng@iphy.ac.cn

specific-heat peak. The magnetically ordered state below T_C was identified as a splayed ferromagnetic (SF) structure with the Yb^{3+} moments of $\sim 1.1\,\mu_B$ pointing along but slightly deviating from a common fourfold cubic axis as a result of the dominant Ising-like ferromagnetic exchange interactions competing with the local XY anisotropy [16]. Within the ferromagnetically ordered state below T_C, however, persistent spin dynamics has been confirmed by a variety of microscopic experimental techniques, which reveal a first-order drop of the spin fluctuation rate by a factor of 10^2-10^4 Hz, i.e., from gigahertz to megahertz [18]. The quantum fluctuations on top of the geometrical frustration are expected to be responsible for the persistent spin dynamics down to the lowest temperatures. More recently, the first-order transition at T_C in $Yb_2Ti_2O_7$ has been described as a Higgs transition from a high-temperature magnetic Coulomb liquid to a ferromagnet with gapped spin excitations within the framework of a quantum spin ice [15,20]. In striking contrast with the ferromagnetic ground state observed in $Yb_2B_2O_7$ (B = Ti, Sn), we recently found that the chemically pressurized $Yb_2Ge_2O_7$ obtained under HPHT conditions undergoes a second-order antiferromagnetic transition at $T_N = 0.62$ K [21] and adopts a ψ_2 or ψ_3 spin structure favored by the OBD mechanism for the XY pyrochlores [12]. As for $Er_2B_2O_7$, we have also qualitatively explained the evolution of their magnetic ground states in the series of $Yb_2B_2O_7$ (B = Sn,Ti,Ge) by considering the strengthened XY-type exchange interactions $J_\pm$ under chemical pressure [12].

These above-mentioned systematic studies demonstrated that the magnetic ground states of these highly frustrated quantum-spin XY pyrochlores are fragile and are prone to alter under subtle perturbations via a proper selection of the B-site cation. Therefore, synthesis and characterization of more XY-type pyrochlores would permit us to build up a more coherent understanding of these geometrically frustrated quantum spin systems. To further enlarge the family of XY pyrochlores, we have chosen to stabilize the Pt-based cubic pyrochlores under HPHT conditions. On the one hand, Pt^{4+} ($t_{2g}^6 e_g^0$ in a low-spin state) in an octahedral oxygen coordination is nonmagnetic and its ionic radius [22] (0.625 Å) is located in between those of Ti^{4+} (0.605 Å) and Sn^{4+} (0.69 Å), allowing us to further verify the effect of chemical pressure. On the other hand, unlike the previously studied $R_2B_2O_7$ with the B site occupied by either a $3d$ transition metal like Ti or a p-block metal such as Ge and Sn, the Pt^{4+} has spatially more extended $5d$ orbitals and thus enhanced Pt $5d$-$O2p$ hybridizations that might modify the local anisotropic exchange interactions. Such an effect has not been taken into account in previous studies. The HPHT syntheses of cubic $R_2Pt_2O_7$ pyrochlores were reported in 1968 by Hoekstra and Gallagher [23], but their magnetic properties have not been characterized so far to the best of our knowledge.

Here, we have prepared the cubic pyrochlores $Er_2Pt_2O_7$ and $Yb_2Pt_2O_7$ under 4 GPa and 1000 °C, and characterized their magnetic properties via measurements of dc and ac magnetic susceptibility and specific heat down to 70 mK. We found that both compounds enter a long-range magnetically ordered state below a similar transition temperature of $T_{N,C} \approx 0.3$ K. Based on the field dependence of their transition temperatures and systematic comparisons of the characteristics with their respective analog compounds $R_2B_2O_7$ (R = Er, Yb; B = Sn, Ti, Ge), we have ascribed the magnetic transition to an antiferromagnetic and a ferromagnetic type for $Er_2Pt_2O_7$ and $Yb_2Pt_2O_7$, respectively. The observed T_N of $Er_2Pt_2O_7$ is much lower than that expected from the relationship of T_N versus the ionic radius (IR) of B^{4+} for the series of $Er_2B_2O_7$, while the T_C of $Yb_2Pt_2O_7$ is the highest among the ferromagnetic $Yb_2B_2O_7$ (B = Sn, Pt, Ti) compounds. Given the monotonic variation of the lattice constant as a function of the B-cation size across these two series of $R_2B_2O_7$ (R = Er, Yb), the observed anomalous $T_{N,C}$ values in the Pt-based XY pyrochlores imply that another important factor beyond the effect of chemical pressure is playing a role. Taking $R_2Pt_2O_7$ (R = Er and Yb) together within the framework of XY pyrochlores with anisotropic exchange interactions J_{ex}, we propose that these abnormal values of $T_{N,C}$ should be attributed to a suppressed (enhanced) antiferromagnetic planar $J_\pm$ (ferromagnetic Ising-like J_{zz}) due to strong Pt $5d$-$O2p$ hybridizations within the plane perpendicular to the local [111] direction. The local structural parameters extracted from the neutron powder diffraction support such a scenario.

II. EXPERIMENT

HPHT synthesis is required to stabilize the Pt-based rare-earth pyrochlores since PtO_2 has a low melting point at ambient pressure. Following previous work [23], the cubic $R_2Pt_2O_7$ (R = Er, Yb) pyrochlores in the present study were prepared under 4 GPa and 1000 °C by using a Kawai-type multianvil module (Max Voggenreiter GmbH) in the Institute of Physics, Chinese Academy of Sciences. The starting materials were high-purity R_2O_3 and PtO_2 mixed in a stoichiometric ratio. As reported earlier [23], the resultant high-pressure products contain a certain amount of platinum metal and unreacted R_2O_3, which can be removed by solution in warm aqua regia. To facilitate the magnetic and specific-heat measurements, the obtained powders, after washing several times in deionized water, were then pressed into pellets and subjected to heat treatment at 900 °C for 10 h in air at ambient pressure.

The phase purity of the powder and pellet samples was examined by powder x-ray diffraction (XRD) or neutron powder diffraction (NPD) at room temperature. Structural parameters were extracted from the XRD/NPD patterns via Rietveld refinement with the FULLPROF program. The NPD measurement was carried out with the neutron powder diffractometer HB-2A at the High Flux Isotope Reactor (HFIR) of the Oak Ridge National Laboratory (ORNL), with the wavelength $\lambda = 1.5405$ Å and collimation of 12′-open-6′. The dc magnetic susceptibility was measured with a commercial magnetic properties measurement system (MPMS-III, Quantum Design) in the temperature range from 1.8 to 300 K under an external magnetic field of $\mu_0 H = 0.1$ T. Ac magnetic susceptibility measurements down to 70 mK were performed in an Oxford dilution refrigerator with the mutual induction method; an excitation current of ~ 1 mA with a frequency of 317 Hz was applied to the primary coil during the measurements. Specific-heat data in the temperature range from 70 mK to 300 K were collected with a physical properties measurement system (PPMS, Quantum Design) equipped with a dilution refrigerator insert.

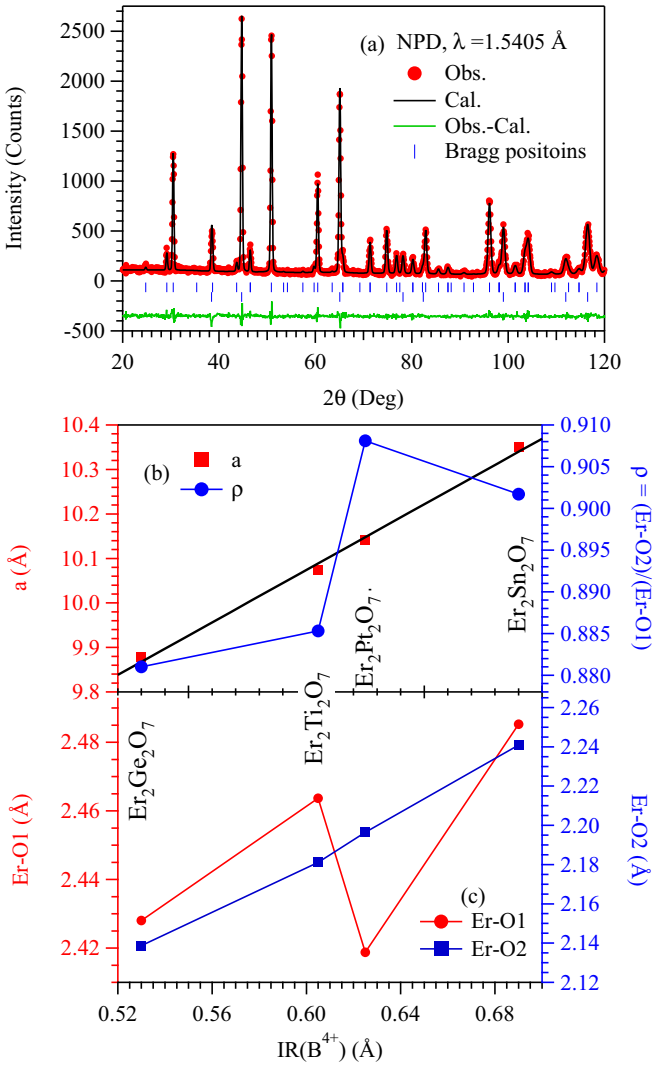

FIG. 1. (a) NPD pattern of $Er_2Pt_2O_7$ at room temperature and the result of Rietveld refinement. The two series of allowed Bragg reflections correspond to the main cubic pyrochlore phase and the aluminum metal from the sample holder. (b) Lattice parameter a and the Er-O bond length ratio $\rho \equiv$ (Er-O2)/(Er-O1) characterizing the axial distortion of ErO_8 polyhedra, and (c) Er-O bond lengths in the series of $Er_2B_2O_7$ (B = Sn, Pt, Ti, Ge) as a function of the ionic radius (IR) of the B^{4+} ions.

III. RESULTS AND DISCUSSION

A. $Er_2Pt_2O_7$

The XRD pattern of the $Er_2Pt_2O_7$ sample after heat treatment at 900 °C for 10 h at ambient pressure indicated that the obtained sample is single phase with the cubic pyrochlore structure. To extract reliable structural information, we measured the NPD spectrum and performed Rietveld refinements in a cubic $Fd\bar{3}m$ (no. 227) space group with the Er atom at the 16d (1/2,1/2,1/2), the Pt atom at the 16c (0,0,0,), the O1 atom at the 48f (x,1/8,1/8), and the O2 atom at the 8b (3/8,3/8,3/8) site, respectively. The refinement converged well as illustrated in Fig. 1(a). The structural parameters of $Er_2Pt_2O_7$ after Rietveld refinements are collected in Table I together with those of $Er_2B_2O_7$ (B = Sn [24], Ti [25], Ge [11]) for comparison. The obtained lattice parameter $a = 10.1448(2)$ Å is in excellent agreement with the previously reported value of 10.144 Å (Ref. [23]), and falls on the straight line of a versus the IR of the B^{4+} ions for the series of $Er_2B_2O_7$ as shown in Fig. 1(b).

In contrast with the monotonic variation of the global lattice parameter as a function of the IR of B^{4+}, the local coordination environment around the Er^{3+} ions was found to exhibit pronounced modification for $Er_2Pt_2O_7$. In our previous work [11], we introduced an Er-O bond length ratio $\rho \equiv$ (Er-O2)/(Er-O1) to characterize the axial distortion along the local [111] direction, and it was observed that ρ increases gradually with the IR of the B^{4+} ions in the series of $Er_2B_2O_7$ (B = Ge, Ti, Sn). Interestingly, we observed an unusually large ρ for $Er_2Pt_2O_7$ as illustrated in Fig. 1(b). The large ρ likely arises from a relatively short Er-O1 bond which lies roughly within the buckled plane perpendicular to the local [111] direction (inset of Fig. 5). As can be seen clearly in Fig. 1(c), the Er-O1 bond length indeed displays an anomalous drop at $Er_2Pt_2O_7$, while the Er-O2 bond length increases almost linearly with the IR of B^{4+}. The observation of such an anisotropic modification on the local coordination environment of Er^{3+} ions is quite unexpected, and might reflect an intrinsic crystallographic feature associated with the Pt^{4+} ions having spatially more extended 5d orbitals. As discussed below, the observed unusual magnetic properties in the XY pyrochlores might be attributed to this anisotropic local structural change.

Figure 2(a) displays the temperature dependence of the dc magnetic susceptibility $\chi(T)$ and its inverse $\chi^{-1}(T)$ for $Er_2Pt_2O_7$ measured under $\mu_0 H = 0.1$ T after zero-field cooling (ZFC) from room temperature. No anomaly signaling a long-range magnetic order was observed down to 1.8 K. A Curie-Weiss (CW) fitting to $\chi^{-1}(T)$ in the temperature range 50–300 K yields an effective moment $\mu_{\rm eff} = 9.86\,\mu_B$ per Er^{3+} and a CW temperature $\theta_{\rm CW} = -22.4$ K. The obtained $\mu_{\rm eff}$ is close to that of $Er_2B_2O_7$ (B = Sn [10], Ti [26], Ge [11]), and is in accordance with the expected value of 9.58 μ_B for the $^4I_{15/2}$ ground state of Er^{3+}. Although the nearest-neighbor distance between Er^{3+} ions in $Er_2Pt_2O_7$ is located in between those of $Er_2Sn_2O_7$ and $Er_2Ti_2O_7$, the obtained $\theta_{\rm CW} = -22.4$ K is much larger than that of -14.32 K for $Er_2Sn_2O_7$ [10] and -15.93 K for $Er_2Ti_2O_7$ [26]. The unusually large $|\theta_{\rm CW}|$ of $Er_2Pt_2O_7$ can be attributed to the enhanced crystalline electric field (CEF) effect.

Figure 2(b) shows the magnetization curves $M(H)$ of $Er_2Pt_2O_7$ at 2 and 5 K. As can be seen, the $M(H)$ curve at 2 K exhibits a clear slope change around $H_c = 2.5$ T, which increases with temperature. Such a behavior has also been observed in other $Er_2B_2O_7$ pyrochlores [11] and corresponds to a field-induced spin-flop transition to a highly polarized state for $H > H_c$.

In order to search for possible long-range magnetic order in $Er_2Pt_2O_7$, we turn to the results of ac magnetic susceptibility $\chi'(T)$ measured from 2 K down to 70 mK. As shown in Fig. 3, the $\chi'(T)$ curve displays a clear cusplike anomaly at about 0.3 K. In addition, this anomaly does not exhibit noticeable dependence on frequency and magnetic field (up to 0.3 T), signaling the appearance of long-range antiferromagnetic order. Given the close IR between Pt^{4+} (0.625 Å) and Ti^{4+} (0.605 Å), the occurrence of long-range antiferromagnetic order in $Er_2Pt_2O_7$

TABLE I. Comparison of the structural and magnetic properties of the cubic pyrochlores $Er_2B_2O_7$ (B = Ge, Ti, Pt, Sn). AFM indicates antiferromagnetic and NN nearest neighbor. "∼" indicates close to.

$Er_2B_2O_7$	Ge	Ti	Pt	Sn
IR(B^{4+}) (Å)	0.53	0.605	0.625	0.69
a (Å)	9.8782(2)	10.074(1)	10.1448(2)	10.3504(1)
$R_{NN} \equiv [(\sqrt{2}/4)a]$(Å)	3.492	3.562	3.587	3.659
x of O1 at 48f	0.3292(6)	0.331	0.3400(2)	0.3375
Er-O2 (×2) (Å)	2.1387(1)	2.1811	2.1964(2)	2.2409
Er-O1 (×6) (Å)	2.428(3)	2.4637	2.4188(11)	2.4853
$\rho \equiv$ (Er-O2)/(Er-O1)	0.881(1)	0.8853	0.9081	0.9017
$\theta_{CW}(K)$	−21.9	−15.9	−22.4	−14
T_N (K)	1.41	1.17	0.30	
Order type	AFM	AFM	AFM	∼(AFM)
Spin state	ψ_3	ψ_2		∼(PC)
Reference	[11]	[25]	This work	[24]

is expected, but this lower T_N (0.3 K versus ∼1.2 K for $Er_2Ti_2O_7$) is quite unexpected as is discussed below.

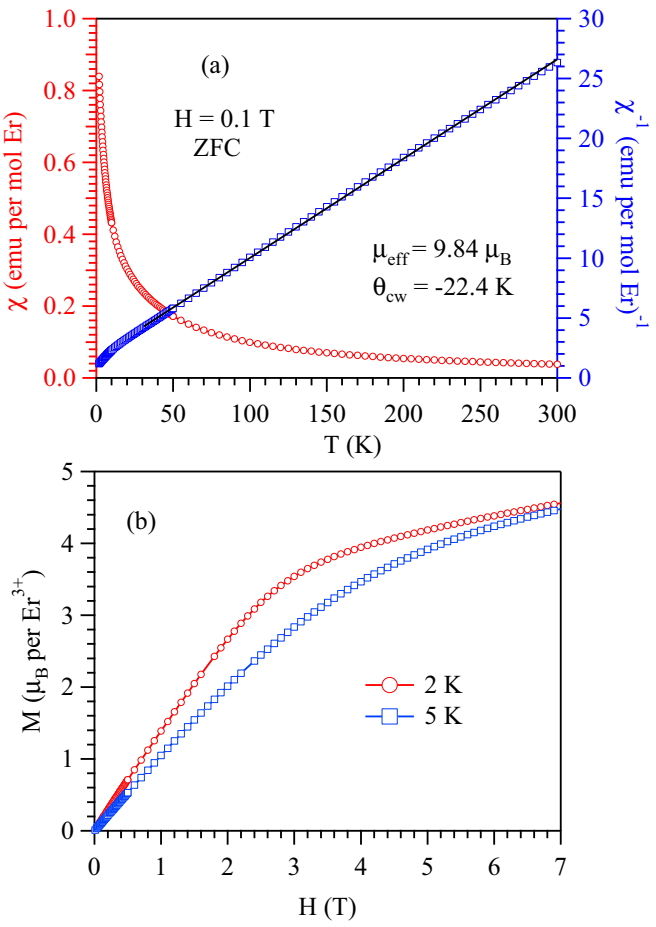

FIG. 2. (a) Temperature dependence of the dc magnetic susceptibility $\chi(T)$ and its inverse $\chi^{-1}(T)$ of $Er_2Pt_2O_7$ measured under 0.1 T in zero-field-cooling (ZFC) mode from 1.8 to 300 K. The solid line represents the Curie-Weiss fitting curve to $\chi^{-1}(T)$ in the temperature range from 50 to 300 K. The obtained effective moment μ_{eff} and Curie-Weiss temperature θ_{CW} are shown in the figure. (b) Magnetization curves of $Er_2Pt_2O_7$ between 0 and 7 T at 2 and 5K.

Figure 4(a) shows the specific heat $C(T)$ of $Er_2Pt_2O_7$ in the temperature range from 70 mK to 50 K under zero magnetic field. As can be seen, the $C(T)$ data plotted in a semilogarithmic scale exhibit a sharp λ-shaped peak at $T_N = 0.3$ K, in excellent agreement with the $\chi'(T)$ data shown in Fig. 3, providing further evidence for the occurrence of a second-order phase transition to an antiferromagnetically ordered state below T_N. In the following, we have employed the procedure previously used for $Er_2Ge_2O_7$ to extract the magnetic contribution C_m and to estimate the entropy associated with the antiferromagnetic transition [11].

Here, we measured the $C(T)$ of an isostructural, non-magnetic $Lu_2Pt_2O_7$ cubic pyrochlore prepared under similar conditions as the lattice standard C_{lat}. Considering the very close molar mass and the negligible contribution below 10 K we did not undertake any mass correction to C_{lat}. After subtracting C_{lat} from the measured C_{total}, we obtained the

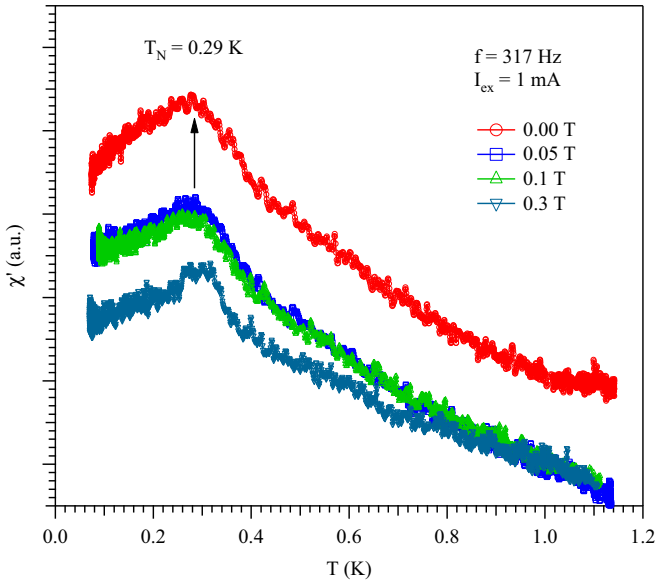

FIG. 3. Temperature dependence of the ac magnetic susceptibility $\chi'(T)$ under different external magnetic fields up to 0.3 T for $Er_2Pt_2O_7$ in the temperature range from 60 mK to 1.1 K.

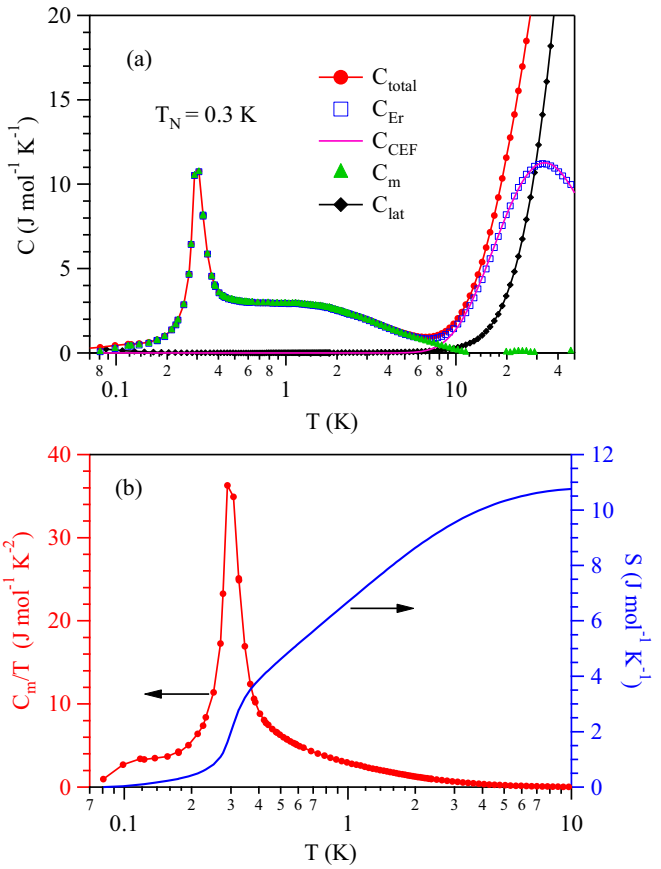

FIG. 4. (a) Temperature dependence of specific heat $C(T)$ of $Er_2Pt_2O_7$. See the text for the analysis. (b) Magnetic specific heat C_m and entropy S associated with the long-range antiferromagnetic transition.

specific-heat contribution from the magnetic Er^{3+} ions, C_{Er}. As shown in Fig. 4(a), the broad hump above 10 K for C_{Er} should be ascribed to the Er^{3+} CEF levels (C_{CEF}), which are expected to split into eight doublets in the D_{3d} symmetry for $Er^{3+}(J = 15/2)$. We found that C_{Er} between 15 and 50 K can be described well by considering the first and the second excited doublets located at 62.0(1) K and 127(1) K, respectively. The first excited doublet agrees in general with those of $Er_2B_2O_7$, i.e., 59.1 K for B = Sn [10], 74 K for B = Ti [3], and 73 K for B = Ge [11].

Finally, C_m is obtained by subtracting C_{CEF} from C_{Er} and is found to dominate the specific heat below 10 K. Figure 4(b) displays the C_m/T and the corresponding entropy S obtained by integrating C_m/T over the investigated temperature range. As can be seen, S reaches a constant value of 10.75 J mol^{-1} K^{-1}, which can account for nearly 93% of the ideal value $2R\ln(2S+1)$ for $S = 1/2$. Such an agreement illustrates that, like other $Er_2B_2O_7$ XY pyrochlores, the Er^{3+} ions with a Kramers doublet ground state in $Er_2Pt_2O_7$ can be described as an effective pseudospin $S = 1/2$. In addition, it was found that a large portion (∼80%) of the entropy is released above $T_N = 0.3$ K, which suggests the existence of significant short-range spin correlations before the compound finally enters the long-range ordered state.

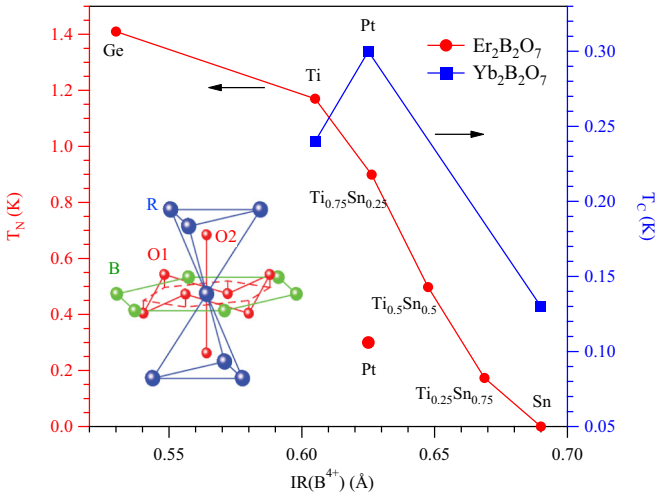

FIG. 5. Variations of T_N (left) and T_C (right) for the XY pyrochlores $Er_2B_2O_7$ (B = Ge, Ti, $Ti_{0.75}Sn_{0.25}$, $Ti_{0.5}Sn_{0.5}$, $Ti_{0.25}Sn_{0.75}$, Sn, and Pt) and $Yb_2B_2O_7$ (B = Sn, Pt, Ti) as a function of the IR of the B^{4+} ions. Inset depicts the local environment of a given rare-earth R atom in the pyrochlore structure (adopted from [Ref. [34]]).

The above detailed characterizations of the cubic $Er_2Pt_2O_7$ confirm that it is an additional XY pyrochlore antiferromagnet with $T_N = 0.3$ K. As mentioned above, the observed T_N is unexpectedly low based on the previous knowledge of the series of $Er_2B_2O_7$ (B = Sn, Ti, Ge) pyrochlores covering a broad range of IR for the B^{4+} ions from 0.53 to 0.69 Å. We have plotted in Fig. 5 the T_Ns of these Er-based XY pyrochlore antiferromagnets $Er_2B_2O_7$ (B = Ge, Ti, $Ti_{0.75}Sn_{0.25}$, $Ti_{0.5}Sn_{0.5}$, $Ti_{0.25}Sn_{0.75}$, Sn, and Pt) as a function of the IR of the B^{4+} ion [27]. As can be seen, T_N of $Er_2Pt_2O_7$ is about 0.6 K lower than that of $Er_2(Ti_{0.75}Sn_{0.25})_2O_7$, in which the combination of $Ti_{0.75}Sn_{0.25}$ has a similar IR as Pt^{4+}. This observation suggests that there are other important factors beyond the nearest-neighbor Er-Er distance that weaken the anisotropic antiferromagnetic exchange interactions or enhance the magnetic frustration in $Er_2Pt_2O_7$. We will come back to this point after we take the magnetic properties of $YbPt_2O_7$ into consideration.

B. $Yb_2Pt_2O_7$

The characterizations of $Yb_2Pt_2O_7$ follow the identical procedures as those done for $Er_2Pt_2O_7$ shown above. Figure 6(a) shows the powder XRD pattern of $Yb_2Pt_2O_7$ after Rietveld refinement, which confirmed that the obtained sample is nearly single phase with the presence of a tiny amount of platinum metal, i.e., ∼1.7(5) wt. % according to the scaling factors. The obtained structural parameters of $Yb_2Pt_2O_7$ after refinements are listed in Table II together with those of $Yb_2B_2O_7$ (B = Sn, Ti, Ge) for comparison. The obtained lattice parameter a = 10.0923(5) Å agrees well with the previously reported value of 10.095Å [23], and scales excellently with the IR of the B^{4+} ions for the series of $Yb_2B_2O_7$ as shown in Fig. 6(b). This observation together with the linearity of a versus the ionic radius of B^{4+} shown in Fig. 1(b) further demonstrates that a proper selection of nonmagnetic B-site cations indeed

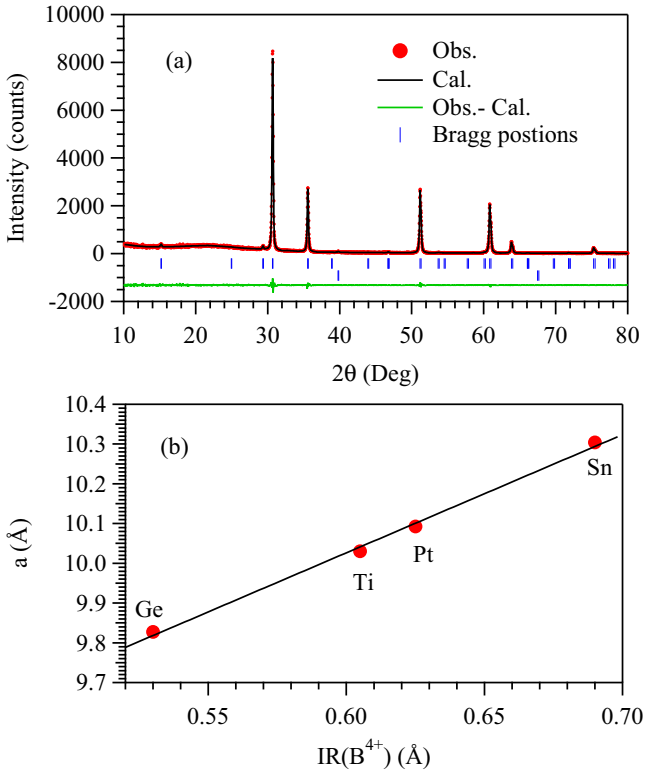

FIG. 6. (a) XRD pattern of $Yb_2Pt_2O_7$ at room temperature and the result of Rietveld refinement. The two series of allowed Bragg reflections correspond to the main cubic pyrochlore phase and the secondary phase of platinum metal. (b) Variation of the lattice constant a as a function of the ionic radius (IR) of the B^{4+} cation for the $Yb_2B_2O_7$ (B = Sn, Pt, Ti, Ge) cubic pyrochlores.

provides a clean means to fine-tune the chemical pressure of the geometrically frustrated rare-earth sublattice.

The main panel of Fig. 7 shows $\chi(T)$ and its inverse $\chi^{-1}(T)$ for $Yb_2Pt_2O_7$ in the temperature range between 1.8 and 300 K measured under $\mu_0 H = 0.1$ T in the ZFC mode. No magnetic ordering was observed down to 1.8 K. As observed in $Yb_2B_2O_7$ (B = Ti, Sn), $\chi^{-1}(T)$ does not follow the CW behavior in the high-temperature region due to the contribution from the excited CEF states. Rather than considering a large temperature-dependent Van Vleck term, we performed a CW fitting to $\chi^{-1}(T)$ below 20 K (inset of Fig. 7) and obtained an effective moment $\mu_{\rm eff} = 3.08\,\mu_{\rm B}$ per Yb^{3+}

TABLE II. Comparison of the structural and magnetic properties of the cubic pyrochlores $Yb_2B_2O_7$ (B = Ge, Ti, Pt, Sn). AFM indicates antiferromagnetic, FM ferromagnetic, SF splayed ferromagnet.

$Yb_2B_2O_7$	Ge	Ti	Pt	Sn
IR(B^{4+}) (Å)	0.53	0.605	0.625	0.69
a (Å)	9.8257(5)	10.032	10.0923	10.304
$\theta_{CW}(K)$	+0.90	+0.75	+0.91	+0.64
$T_{N,C}$(K)	0.62	0.24	0.30	0.15
Order type	AFM	FM	FM	FM
Spin structure	$\psi_{2\,\rm or\,3}$	SF		SF
Reference	[21]	[18]	This work	[16]

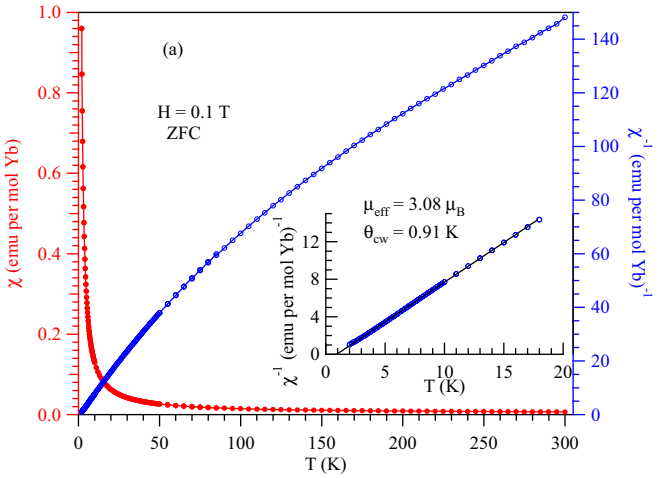

FIG. 7. The temperature dependence of the dc magnetic susceptibility χ(T) and its inverse $\chi^{-1}(T)$ for $Yb_2Pt_2O_7$ measured under 0.1 T after zero-field cooling (ZFC) from 300 K. Inset shows the Curie-Weiss fitting to $\chi^{-1}(T)$ below 20 K.

and a CW temperature $\theta_{\rm CW} = +0.91$ K for $Yb_2Pt_2O_7$. The obtained $\mu_{\rm eff}$ is close to those of other Yb pyrochlores [13,17] and corresponds to a ground doublet average g value of 3.55. The positive $\theta_{\rm CW}$ signals dominant ferromagnetic exchange interactions as observed in $Yb_2B_2O_7$ (B = Ti, Sn). However, it is interesting to note that the obtained $\theta_{\rm CW}$ for $Yb_2Pt_2O_7$ is larger than the typical values of +0.5–0.75 K observed in $Yb_2B_2O_7$ (B = Ti [13,21], Sn [16,17]). The larger $\theta_{\rm CW}$ implies stronger ferromagnetic interactions in $Yb_2Pt_2O_7$, in line with the higher ferromagnetic transition temperature T_C shown below.

To access the possible long-range magnetic order in $Yb_2Pt_2O_7$, we also measured the ac magnetic susceptibility down to 70 mK in a dilution refrigerator. The main panel of Fig. 8 shows (a) the real $\chi'(T)$ and (b) the imaginary $\chi''(T)$ under different external dc magnetic fields $H_{\rm dc}$ up to 0.3 T. As shown in Fig. 8(a), $\chi'(T)$ at $H_{\rm dc} = 0$ T exhibits a rounded peak at about 0.3 K and does not show noticeable frequency dependence, signaling the occurrence of a long-range magnetic order in $Yb_2Pt_2O_7$. With increasing $H_{\rm dc}$, the magnitude of χ'(T) is suppressed gradually, and the peak position shifts to higher temperatures as shown in the inset of Fig. 8(a). These characteristics of $\chi'(T)$ for $Yb_2Pt_2O_7$ quantitatively resemble those observed near the ferromagnetic transitions of $Yb_2B_2O_7$ (B = Ti, Sn), but differ sharply from those of antiferromagnetic $Yb_2Ge_2O_7$ [21]. Specifically, with increasing $H_{\rm dc}$ the magnitude of $\chi'(T)$ is strongly suppressed in the temperature regions both below and above T_C and the peak position moves up for $Yb_2B_2O_7$ (B = Ti, Sn), but the magnitude of $\chi'(T)$ is enhanced below T_N and the peak position shifts slightly down for $Yb_2Ge_2O_7$. From these comparisons, we can conclude that the $\chi'(T)$ peak around 0.3 K for $Yb_2Pt_2O_7$ should correspond to the development of long-range ferromagnetic order as seen in $Yb_2B_2O_7$ (B = Ti, Sn).

$\chi''(T)$ of $Yb_2Pt_2O_7$ also displays below T_C a symmetric peak at T_0, whose position does not vary with $H_{\rm dc}$ but smears out above 0.1 T. In addition, a shoulder first develops around

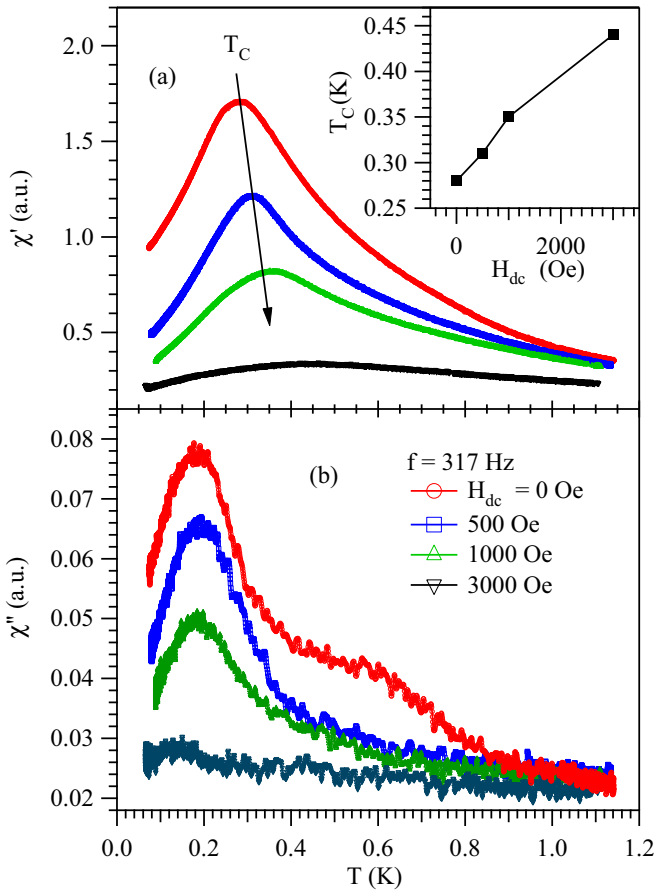

FIG. 8. Temperature dependence of the ac magnetic susceptibility (a) $\chi'(T)$ and (b) $\chi''(T)$ for $Yb_2Pt_2O_7$ measured under different external magnetic fields H_{dc} up to 0.3 T. Inset shows the H_{dc} dependence of T_C.

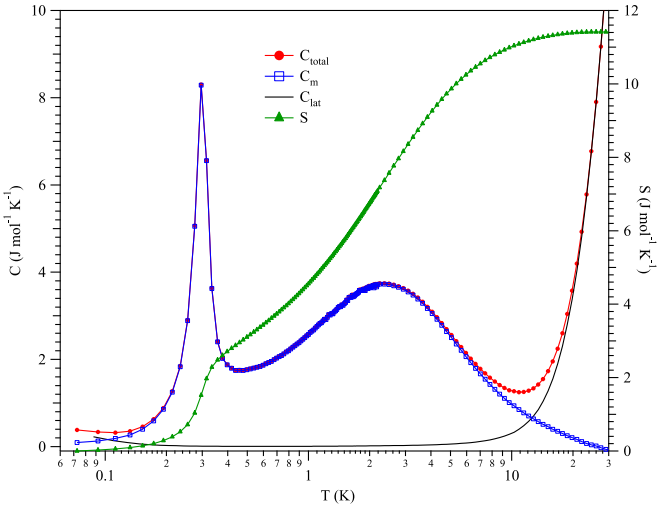

FIG. 9. Temperature dependence of specific heat $C(T)$, the magnetic specific heat C_m, and the entropy S associated with the ferromagnetic transition of $Yb_2Pt_2O_7$. See the text for the analysis.

0.8 K upon cooling for the $\chi''(T)$ under $H_{dc} = 0$ T, and this feature fades away immediately upon the application of H_{dc}. According to recent experimental and theoretical studies on $Yb_2Ti_2O_7$ [28,29], the existence of a possible high-temperature phase transition above T_C under zero field in $Yb_2Pt_2O_7$ might correspond to the ψ_2/ψ_3 OBD transition as a result of SF/U(1) multiphase competition. Such a competition can be removed by the application of an external magnetic field.

The occurrence of long-range magnetic order in $Yb_2Pt_2O_7$ was further confirmed by the ultralow-temperature $C(T)$ measurement. Figure 9 shows the $C(T)$ data of $Yb_2Pt_2O_7$ from 30 K down to 70 mK under zero magnetic field. For the $C(T)$ data plotted on the semilogarithmic scale, two features are clearly noticeable: a sharp λ-shaped peak at $T_C = 0.3$ K and a broad hump centered around 2.5 K. All these features in $C(T)$ quantitatively resemble those observed in the $Yb_2B_2O_7$ (B = Ti, Sn) series [16,18]: the sharp peak at 0.3 K, in excellent agreement with the $\chi'(T)$ data shown in Fig. 8(a), should be ascribed to a first-order transition to a ferromagnetically ordered state below T_C, while the broad anomaly near 2.5 K arises from the Schottky anomaly associated with the exchange splitting of the ground Kramers doublet upon the onset of magnetic correlations. By considering the quantum spin ice Hamiltonian with anisotropic exchange interactions, the latter feature in $Yb_2Ti_2O_7$ was produced by Applegate *et al.* [30] and was suggested to be a crossover from a paramagnetic to a spin ice state. They further suggested that a double-peaked $C(T)$ with an entropy between the peaks of a value comparable to the residual Pauling entropy $S_p = (R/2)\ln(3/2)$ is the hallmark of a quantum spin ice.

In order to evaluate the magnetic entropy associated with the above-mentioned transitions, we have obtained the magnetic C_m by subtracting from the measured total $C(T)$ the lattice contribution C_{lat} given by an isostructural, nonmagnetic $Lu_2Pt_2O_7$. As can be seen in Fig. 9, C(T) of $Lu_2Pt_2O_7$ is nearly identical to that of $Yb_2Ti_2O_7$ at ∼20 K, which suggests that the first excited doublet is located at much higher temperature than that of $Er_2Pt_2O_7$. A preliminary analysis on the C_m data above 100 K suggests that the first excited doublet is located around 700 K, similar to the value of 680 K found in $Yb_2Ti_2O_7$.The magnetic entropy S was obtained by integrating C_m/T over the investigated temperature range and also given in Fig. 9. As can be seen, S reaches a constant value of 11.42 J mol^{-1} K^{-1}, which can account for 99% of the ideal value $2R\ln(2S+1)$ for $S = 1/2$ without any residual entropy. This agreement indicated that, like other Yb pyrochlores, the Yb^{3+} moments in $Yb_2Pt_2O_7$ can be described as an effective $S = 1/2$ pseudospin due to a well-isolated Kramers doublet ground state, supported by the preliminary specific-heat analysis mentioned above. As generally observed in geometrically frustrated magnets, over 80% of the entropy is released above T_C. Although the entropy plateau at S_p cannot be defined unambiguously (a similar situation occurs in the quantum spin ice candidate $Yb_2Ti_2O_7$ [30]), the significant short-range spin correlations before finally entering the long-range ordered state at T_C might be associated with accidental OBD selection of the ψ_2/ψ_3 state [29] or the formation of spin ice configurations according to the quantum spin ice model [30].

Based on the above characterizations, we can conclude that the cubic pyrochlore $Yb_2Pt_2O_7$ develops a long-range

ferromagnetic order below $T_C = 0.3$ K with several characteristics similar with those of well-studied $Yb_2B_2O_7$ (B = Sn, Ti). As mentioned above, since the IR of Pt^{4+} (0.625 Å) is located in between that of Sn^{4+} (0.69Å) and that of Ti^{4+} (0.605Å), the observation of similar ferromagnetic order is not surprising. However, the observed $T_C = 0.3$ K for $Yb_2Pt_2O_7$ is unexpectedly higher than those of $Yb_2Sn_2O_7$ ($T_c = 0.11-0.15$ K) and $Yb_2Ti_2O_7$ ($T_c = 0.21-0.26$ K) as is shown in Fig. 5. The higher θ_{CW} and T_C suggest that the ferromagnetic exchange interactions are enhanced in $Yb_2Pt_2O_7$ among these Yb-based pyrochlores. Similarly, such an enhancement cannot be simply attributed to the effect of chemical pressure in that the lattice constant follows a monotonic variation as a function of the B-cation size across the series of $Yb_2B_2O_7$ (B = Ti, Pt, Sn) as shown in Fig. 6(b).

IV. DISCUSSION

From the above results, we can see that the magnetic properties of $Er_2Pt_2O_7$ and $Yb_2Pt_2O_7$ follow the general characteristics of the respective series of $Er_2B_2O_7$ and $Yb_2B_2O_7$. Considering the similar IR of Pt^{4+} (0.625 Å) and Ti^{4+}(0.605 Å), both the antiferromagnetic order in $Er_2Pt_2O_7$ and the ferromagnetic order in $Yb_2Pt_2O_7$ have one-to-one counterparts in the corresponding Ti-based pyrochlores. These observations are not surprising in that the replacement of nonmagnetic Pt^{4+} is not expected to modify significantly the single-ion anisotropy and the leading term among the anisotropic exchange interactions J_{ex}. This implies that to first order the chemical pressure, or the nearest-neighbor distance, should still play a dominant role in determining the magnetic ground state of these XY pyrochlores.

After resolving the magnetic structures of $Er_2Ge_2O_7$ and $Yb_2Ge_2O_7$ with neutron diffraction [12], we have successfully unified the evolutions of the magnetic ground states for these effective $S = 1/2$ XY pyrochlores $R_2B_2O_7$ (R = Er, Yb; B = Sn, Ti, Ge) in a coherent picture by considering that increasing chemical pressure enhances $J_\pm$ among the anisotropy exchange interactions J_{ex}. In terms of the proposed phase diagrams and the effect of chemical pressure only, $Er_2Pt_2O_7$ should adopt a ψ_2 structure, but closer than $Er_2Ti_2O_7$ to the ψ_2/ψ_4 phase boundary, or adopt a ψ_4 structure instead, while $Yb_2Pt_2O_7$ should adopt a splayed ferromagnetic structure. It should be noted that although the PC correlations have been identified in $Er_2Sn_2O_7$ [31], a static PC ψ_4 state remains unknown among the Er-based XY pyrochlores. In addition to the Heisenberg pyrochlore antiferromagnet $Gd_2Sn_2O_7$ [32], $Er_2Pt_2O_7$ might be another candidate to realize such a state which was proposed theoretically years ago [33]. Thus, further neutron scattering experiments are needed to determine the exact forms of magnetic structure and to confirm the XY character for each case.

Despite the general agreement with expectations for the magnetic ground states of these two XY pyrochlores, the transition temperatures of both Pt-based pyrochlores deviate obviously from the expected behavior, as noted above. As shown in Fig. 5, the antiferromagnetic T_N of $Er_2Pt_2O_7$ is unexpectedly low whereas the ferromagnetic T_C of $Yb_2Pt_2O_7$ is unusually high given the monotonic variation of lattice constant as a function of IR of the B^{4+} cations. These observations suggest that another important factor beyond the nearest-neighbor distance can influence the magnitude of the anisotropic exchange interactions and thus the transition temperatures $T_{N,C}$ for these XY pyrochlores.

Recent studies on $R_2Ti_2O_7$ have illustrated that the magnetic ordering process and the transition temperatures are very sensitive to the chemical stoichiometry or disorder. For example, $Yb_2Ti_2O_7$ single crystals grown by the high-temperature optical floating zone technique were found to exhibit much lower T_C with a suppressed specific-heat anomaly, whereas the polycrystalline samples always display higher T_C and a pronounced $C(T)$ peak [34,35]. Such an extrinsic effect is unlikely to play an important role in the present study. On the one hand, all samples are polycrystalline and prepared under HPHT conditions; refinements on the XRD/NPD patterns in a partially disordered structural model do not give a clear improvement. On the other hand, the $C(T)$ peak is found to be as sharp as those observed in the high-quality $Yb_2Ti_2O_7$ samples. In addition, the enhancement of T_C in $Yb_2Pt_2O_7$ does not support the disorder scenario. Exclusion of the extrinsic effect thus leads us to ask the following: (i) whether the Pt^{4+} ion has some peculiarity compared with other nonmagnetic B^{4+} ions, and (ii) whether we can understand the anomalous $T_{N,C}$ of these two effective $S = 1/2$ XY pyrochlores in a unified picture?

In striking contrast with the previously studied $R_2B_2O_7$ with the B site occupied with either a $3d$ transition metal like Ti or a p-block metal such as Ge and Sn, the B sites of $R_2Pt_2O_7$ (R = Er, Yb) pyrochlores are occupied by the $5d$ transition metal Pt^{4+} in a low-spin configuration t^6e^0. As pointed out in the Introduction, it not only has spatially more extended $5d$ orbitals than the $3d$ counterparts, but also can enhance the Pt $5d$-$O2p$ hybridizations via the empty e_g orbitals compared to the p-block metals. Such distinct characteristics of the Pt^{4+} ion might modify the relative magnitude of the anisotropic exchange interactions J_{ex}. After pointing out the peculiarities of Pt^{4+}, we are finally in a position to discuss the possible implications from the current study.

As mentioned above, the magnetic ground states of $Er_2B_2O_7$ and $Yb_2B_2O_7$ can be understood within the framework of generalized effective $S = 1/2$ XY pyrochlores with anisotropic exchange interactions J_{ex} [8]; the leading term is the XY planar $J_\pm$ for Er pyrochlores and the Ising-like J_{zz} for Yb pyrochlores. For example, $J_{zz}/J_\pm \approx -0.5$ for $Er_2Ti_2O_7$ and $J_{zz}/J_\pm \approx +3$ for $Yb_2Ti_2O_7$ have been obtained from inelastic neutron scattering. The pronounced reduction of T_N for $Er_2Pt_2O_7$, Fig. 5, implies that the planar $J_\pm$ is weakened to first order. As depicted in the inset of Fig. 5, a given R atom is surrounded by six O1 atoms in a buckled plane perpendicular to the local [111] direction and two O2 atoms on each side of this plane along [111]. Since the planar $J_\pm$ is expected to be mediated by the six in-plane O1 atoms, it is highly possible that the observed weakening of $J_\pm$ is associated with the anisotropic structural modification shown in Figs. 1(b) and 1(c), i.e., the anomalous short Er-O1 bond length. However, it is hard to rationalize why shorter Er-O1 distances in $Er_2Pt_2O_7$ are detrimental to the planar $J_\pm$. Instead, there could be another underlying factor controlling both the structural and magnetic properties. As seen in Fig. 5, the transition-metal B ions also form a hexagon in the same plane

normal to the local [111] direction. The large spatial extension of the Pt^{4+} $5d$ orbitals are thus expected to push away the nearby oxygen atoms so as to explain the short Er-O1 bond length. At the same time, the empty e_g orbitals of Pt^{4+} might hybridize strongly with the O $2p$ orbitals so as to interrupt the mediating power of oxygen between the nearby Er^{3+} moments, leading to a weaken planar $J_{\pm}$ and reduced T_N. If a similar situation takes place in $Yb_2Pt_2O_7$, the reduced $J_{\pm}$ then corresponds to an effective enhancement of J_{zz}, or $J_{zz}/J_{\pm}$, which can explain the observed unusually high T_C in $Yb_2Pt_2O_7$.

V. CONCLUSION

In summary, we have obtained the cubic pyrochlores $Er_2Pt_2O_7$ and $Yb_2Pt_2O_7$ under 4 GPa and 1000 °C, and performed detailed characterizations of their structural and magnetic properties via measurements of XRD/NPD, dc and ac magnetic susceptibility, and specific heat down to 70 mK. Both compounds are effective pseudospin $S = 1/2$ XY pyrochlores with a Kramers doublet ground state. We confirmed that both compounds enter a long-range magnetically ordered state below $T_{N,C} \approx 0.3$K, which have been ascribed to an antiferromagnetic and a ferromagnetic type for $Er_2Pt_2O_7$ and $Yb_2Pt_2O_7$, respectively, based on systematic comparisons with their respective analog compounds $R_2B_2O_7$ (R = Er, Yb; B = Sn, Ti, Ge). Although their magnetic ground states can be generally understood based on the effect of chemical pressure, their transition temperatures exhibit nonmonotonic variations as a function of the IR of the B^{4+} cations. Taking into account the local structural features, we proposed that the observed anomalous $T_{N,C}$ in the Pt-based pyrochlores arises from the strong Pt $5d$-$O2p$ hybridizations within the plane perpendicular to the local [111] direction, which weakens (effectively strengthens) the XY planar antiferromagnetic $J_{\pm}$ (Ising-like ferromagnetic J_{zz}). Our present study thus underscores an important fact of nonmagnetic Pt^{4+} ions beyond the steric effect. Neutron scattering experiments are planned to determine the spin structures and to confirm the XY characters of the R^{3+} ions in $Er_2Pt_2O_7$ and $Yb_2Pt_2O_7$.

ACKNOWLEDGMENTS

This work is supported by the National Science Foundation of China (Grants No. 11304371 and No. 11574377), the National Basic Research Program of China (Grant No.2014CB921500), the Strategic Priority Research Program (B) of the Chinese Academy of Sciences (Grant No. XDB07020100), and the Opening Project of Wuhan National High Magnetic Field Center (Grant No. 2015KF22), Huazhong University of Science and Technology. Z.L.D. and H.D.Z. acknowledge the support of Grant No. NSF-DMR-1350002. J.B.G. and J.S.Z. acknowledge the support of NSF-DMR 1122603. Research conducted at HFIR, ORNL was sponsored by the Scientific User Facilities Division, Office of Basic Energy Sciences, U.S. Department of Energy.

[1] J. S. Gardner, M. J. P. Gingras, and J. E. Greedan, Rev. Mod. Phys. **82**, 53 (2010).
[2] L. Balents, Nature (London) **464**, 199 (2010).
[3] J. D. M. Champion *et al.*, Phys. Rev. B **68**, 020401(R) (2003).
[4] S. T. Bramwell, M. J. P. Gingras, and J. N. Reimers, J. Appl. Phys. **75**, 5523 (1994).
[5] J. P. C. Ruff *et al.*, Phys. Rev. Lett. **101**, 147205 (2008).
[6] M. E. Zhitomirsky, M. V. Gvozdikova, P. C. W. Holdsworth, and R. Moessner, Phys. Rev. Lett. **109**, 077204 (2012).
[7] L. Savary, K. A. Ross, B. D. Gaulin, J. P. C. Ruff, and L. Balents, Phys. Rev. Lett. **109**, 167201 (2012).
[8] A. W. C. Wong, Z. Hao, and M. J. P. Gingras, Phys. Rev. B **88**, 144402 (2013).
[9] J. Lago, T. Lancaster, S. J. Blundell, S. T. Bramwell, F. L. Pratt, M. Shirai, and C. Baines, J. Phys.: Condens. Matter **17**, 979 (2005).
[10] P. M. Sarte, H. J. Silverstein, V. W. B. T. K., J. S. Gardner, Y. Qiu, H. D. Zhou, and C. R. Wiebe, J. Phys.: Condens. Matter **23**, 382201 (2011).
[11] X. Li *et al.*, Phys. Rev. B **89**, 064409 (2014).
[12] Z. L. Dun *et al.*, Phys. Rev. B **92**, 140407(R) (2015).
[13] J. A. Hodges, P. Bonville, A. Forget, M. Rams, K. Krolas, and G. Dhalenne, J. Phys.: Condens. Matter **13**, 9301 (2001).
[14] K. A. Ross, L. Savary, B. D. Gaulin, and L. Balents, Phys. Rev. X **1**, 021002 (2011).
[15] L. Savary and L. Balents, Phys. Rev. Lett. **108**, 037202 (2012).
[16] A. Yaouanc *et al.*, Phys. Rev. Lett. **110**, 127207 (2013).
[17] Z. L. Dun, E. S. Choi, H. D. Zhou, A. M. Hallas, H. J. Silverstein, Y. Qiu, J. R. D. Copley, J. S. Gardner, and C. R. Wiebe, Phys. Rev. B **87**, 134408 (2013).
[18] J. A. Hodges *et al.*, Phys. Rev. Lett. **88**, 077204 (2002).
[19] Y. Yasui *et al.*, J. Phys. Soc. Jpn. **72**, 3014 (2003).
[20] L.-J. Chang, S. Onoda, Y. Su, Y.-J. Kao, K.-D. Tsuei, Y. Yasui, K. Kakurai, and M. R. Lees, Nat. Commun. **3**, 992 (2012).
[21] Z. L. Dun *et al.*, Phys. Rev. B **89**, 064401 (2014).
[22] R. D. Shannon, Acta Crystallogr., Sect. A: Cryst. Phys., Diffr., Theor. Gen. Crystallogr. **32**, 751 (1976).
[23] H. R. Hoekstra and F. Gallagher, Inorg. Chem. **7**, 2553 (1968).
[24] B. J. Kennedy, B. A. Hunter, and C. J. Howard, J. Solid State Chem. **130**, 58 (1997).
[25] Y. Tabira, R. L. Withers, L. Minervini, and R. W. Grimes, J. Solid State Chem. **153**, 16 (2000).
[26] S. T. Bramwell, M. N. Field, J. J. Harris, and I. P. Parkin, J. Phys.: Condens. Matter **12**, 483 (2000).
[27] See S. Masae and B. Steven, ILL Experimental Report No. 5-31-1496 for the T_N's of the $Er_2(Ti_{1-x}Sn_x)_2O_7$.
[28] E. Lhotel, S. R. Giblin, M. R. Lees, G. Balakrishnan, L.-J. Chang, and Y. Yasui, Phys. Rev. B **89**, 224419 (2014).
[29] L. D. C. Jaubert, O. Benton, J. G. Rau, J. Oitmaa, R. R. P. Singh, N. Shannon, and M. J. P. Gingras, Phys. Rev. Lett. **115**, 267208 (2015).
[30] R. Applegate, N. R. Hayre, R. R. P. Singh, T. Lin, A. G. R. Day, and M. J. P. Gingras, Phys. Rev. Lett. **109**, 097205 (2012).

[31] S. Guitteny, S. Petit, E. Lhotel, J. Robert, P. Bonville, A. Forget, and I. Mirebeau, Phys. Rev. B **88**, 134408 (2013).

[32] A. S. Wills, M. E. Zhitomirsky, B. Canals, J. P. Sanchez, P. Bonville, P. Dalmas de Reotier, and A. Yaouanc, J. Phys.: Condens. Matter **18**, L37 (2006).

[33] S. E. Palmer and J. T. Chalker, Phys. Rev. B **62**, 488 (2000).

[34] A. Yaouanc, P. Dalmas de Reotier, C. Marin, and V. Glazkov, Phys. Rev. B **84**, 172408 (2011).

[35] K. A. Ross, T. Proffen, H. A. Dabkowska, J. A. Quilliam, L. R. Yaraskavitch, J. B. Kycia, and B. D. Gaulin, Phys. Rev. B **86**, 174424 (2012).